Spectral Broadening of Ion Bernstein Wave Due to Parametric Decay Instabilities

You may also be interested in:

Excitation of Zonal Flows by ion-temperature-gradient Modes Excited by the Fluid Resonance
Wang Guan-Qiong, Ma Jun, J. Weiland et al.

Results of ICRF Heating Experiments from the EAST 2010 Campaign
HE Zhongxin, ZHANG Xinjun, ZHAO Yanping et al.

Energetic Ion Effects on the Ion Saturation Current*
Bin-Bin Lin, Nong Xiang, Jing Ou et al.

A Tangentially Visible Fast Imaging System on EAST
Jia Manni, Yang Qingquan, Zhong Fangchuan et al.

Q-Band X-Mode Reflectometry and Density Profile Reconstruction
Qu Hao, Zhang Tao, Zhang Shoubiao et al.

Plasma heating effects in the presence of a parametric decay instability
B E Keen and W H W Fletcher

A novel mechanism of low-threshold absolute parametric decay instability of a wave beam
A. Yu. Popov and E. Z. Gusakov

Particle-in-cell simulations of parametric decay instability of radiofrequency wave in the ion cyclotron range of frequency in an inhomogeneous plasma
Chunyun Gan, Nong Xiang, Jing Ou et al.

Observation of PDI on HT-7
J Li, Y Bao, Y P Zhao et al.

Spectral Broadening of Ion Bernstein Wave Due to Parametric Decay Instabilities *

Chun-Yun Gan(甘春芸)[1,2]**, Nong Xiang(项农)[1,2], Zhi Yu(于治)[1,2]

[1]*Institute of Plasma Physics, Chinese Academy of Sciences, Hefei 230031*
[2]*Center for Magnetic Fusion Theory, Chinese Academy of Sciences, Hefei 230031*

The parametric decay instabilities (PDIs) of ion Bernstein wave with different input power levels are investigated via particle-in-cell simulation. It is found that the number of decay channels increases with the input power. Resonant mode–mode couplings dominate for a low input power. With increasing the input power, the nonresonant PDIs appear to dissipate the energy of the injected wave and give rise to edge ion heating. The generated child waves couple with each other as well as the injected wave and/or act as a pump wave to excite new decay channels. As a result, the frequency spectrum is broadened with the increase of the input power.

The parametric decay instabilities (PDIs) have been detected in many tokamaks during the heating scenarios of an rf wave in the ion cyclotron range of frequency (ICRF).[1−8] In some of these experiments, the occurrences of nonresonant parametric decay processes are invoked to interpret the ion heating and/or ion tail formation in the edge region.[2,4−8] Theoretically, the nonresonant parametric decay processes are predicted to occur according to the calculation of their growth rates and thresholds, and the child waves produced in these nonresonant PDIs may lead to ion heating.[9,10] Numerically, the particle-in-cell (PIC), fluid and hybrid models have been successfully used to investigate the parametric decay processes in a wide range of frequencies.[11−18] In Refs. [14,15] the evidence that the ion cyclotron quasimode (ICQM) produced by the nonresonant decay process leads to the increase of kinetic energy of ions is shown. In addition to the ICQMs, the propagating child waves produced by the resonant or nonresonant PDI processes also dissipate the energy of the injected wave. However, the behavior of PDIs of the ICRF wave with different input powers receives slight concern. How the PDI processes develop and dissipate the energy of the injected high power ICRF wave is not well understood.

To explore this energy dissipation process, the PIC method implemented in VSim (VORPAL) software[19] has been used to study the dependence of PDI processes of ICRF on input power. To reveal these effects in relevant experiments, we choose the plasma parameters close to those of the ion Bernstein wave (IBW) heating experiments on HT-7 tokamak.[1,14] It is demonstrated that more decay channels appear and the frequency spectra broaden as the input power is increased. The characteristics of the spectral broadening and how this broadening comes out will be presented.

For simplicity, a plasma with a single ion species, hydrogen, is taken into account. The ion and electron temperatures are 30 eV and 50 eV, respectively. We take the computational domain as follows. The simulation size $l_x = 0.06$ m. The plasma density profile is $n(x) = n_0(0.43 \arctan(5x/l_x - 2) + 0.47)$ with $n_0 = 2 \times 10^{17}$ m^{-3}. The injected wave with the frequency ω_0 is launched by a perturbation current with the form $J(x,t) = J_0(1 - e^{-\gamma t})^2 e^{-(x-0.006)^2/0.006^2} \sin(\omega_0 t)$, where $\gamma = 0.02\omega_0$. The perturbation current amplitude J_0 denotes the level of input power. Typically, $J_0 = 6 \times 10^2$ Am^{-2} corresponds to the input power of roughly one hundred kilowatts. The external magnetic field is constant in the y-direction (toroidal direction in a tokamak geometry) and the cyclotron frequency of hydrogen satisfies $\Omega_H \simeq 0.57\omega_0$ in the simulation region.

In Fig. 1, the spectral energy density $|E_x|^2$ for four typical perturbation amplitudes $J_0 = (6, 9, 12, 24) \times 10^2$ Am^{-2} are plotted versus the normalized frequency at $x = 0.023$ m and $t = 406/\omega_0$. As the input power increases, the broadening of the frequency spectra is clearly demonstrated. In Fig. 1(a), the second and third harmonic modes of the driving frequency are detected in the $J_0 = 6 \times 10^2$ Am^{-2} case. It has been indicated in Ref. [14] that the second and third harmonic modes of the driving frequency are generated by the resonant parametric decay channels $\omega_0 + \omega_0 \rightarrow 2\omega_0$ and $\omega_0 + 2\omega_0 \rightarrow 3\omega_0$, respectively. Meanwhile, a strong zero-frequency component is also present in the spectrum, which may be produced by the self-interaction of the injected wave.[13,14,20] For a low input power in this level, the resonant mode–mode couplings dominate.

As the amplitude of the perturbation current is increased to $J_0 = 9 \times 10^2$ Am^{-2}, new peaks with frequencies $0.57\omega_0$, $1.43\omega_0$ and $1.86\omega_0$ appear in the spectrum as shown in Fig. 1(b). When the perturbation current amplitude rises to a higher level at $J_0 = 12 \times 10^2$ Am^{-2}, the waves observed in the $J_0 = 9 \times 10^2$ Am^{-2} case are also present, together

with a new sideband occurring at frequency $2.43\omega_0$ (Fig. 1(c)). Except for the frequencies mentioned above, the peaks of $1.6\omega_0$ and $4\omega_0$ add to the spectrum of the $J_0 = 24 \times 10^2 \, \mathrm{Am}^{-2}$ case, as shown in Fig. 1(d). However, how these sidebands are generated is unclear. The temporal evolution of the frequency spectrum and the distribution of particles in phase space are helpful to identify the generation mechanism of these frequency peaks. To explain the decay pattern of these observed frequency peaks, we take the $J_0 = 12 \times 10^2 \, \mathrm{Am}^{-2}$ case for instance.

Figure 2 shows the history of the contours of the amplitude of electric field $|E|$ in the x–ω plane and the normalized kinetic energy of ions in the perpendicular direction for the $J_0 = 12 \times 10^2 \, \mathrm{Am}^{-2}$ case. At an early stage in Fig. 2(a), only the injected wave is generated in the simulation. As the injected wave passes through the coupling point where the match condition of wavenumber $k_{2\omega_0} = 2k_{\omega_0}$ is satisfied, the second harmonic wave is generated nearby (Fig. 2(b)). Thereafter, the amplitude of the second harmonic wave grows and other sidebands with frequencies $0.86\omega_0$, $1.14\omega_0$, $1.43\omega_0$, $1.86\omega_0$ and $3.0\omega_0$ appear in the spectrum, as shown in Fig. 2(c). Simultaneously, the ions are heated in the vertical direction as displayed in
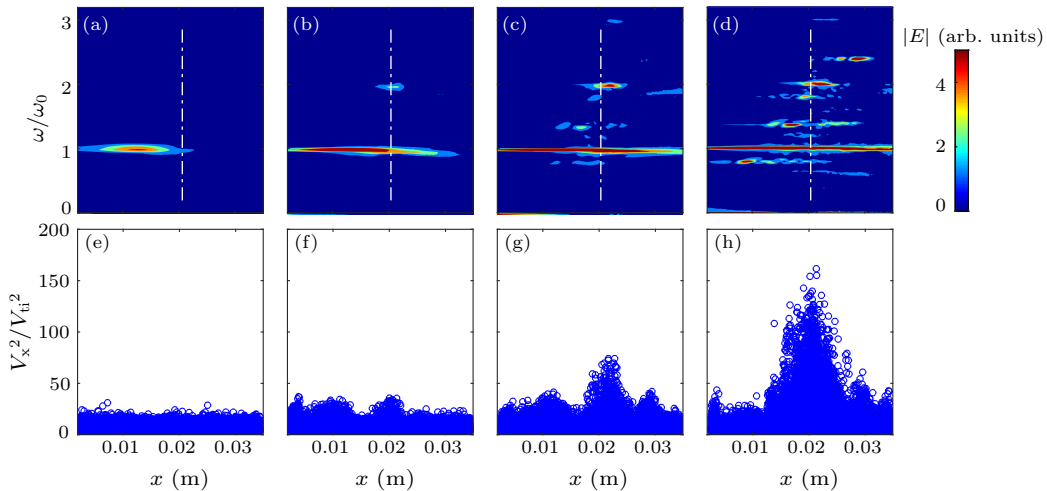
Fig. 2(g). No heating is observed in the parallel direction for ions and in all the directions for electrons. Since there is no ion cyclotron resonance layer located in our simulation region, we conjecture that the ion heating is caused by the nonresonant parametric decay process as presented in Refs. [14,15].

Fig. 1. The frequency spectrum at $x = 0.023 \, \mathrm{m}$ and $t = 406/\omega_0$ in the simulations with different amplitudes of perturbation current: (a) $J_0 = 6 \times 10^2 \, \mathrm{Am}^{-2}$, (b) $J_0 = 9 \times 10^2 \, \mathrm{Am}^{-2}$, (c) $J_0 = 12 \times 10^2 \, \mathrm{Am}^{-2}$ and (d) $J_0 = 24 \times 10^2 \, \mathrm{Am}^{-2}$.

Fig. 2. Contours of the amplitude of $|E|$ in the x–ω plane for the $J_0 = 12 \times 10^2 \, \mathrm{Am}^{-2}$ case at (a) $t = 65/\omega_0$, (b) $t = 122/\omega_0$, (c) $t = 203/\omega_0$ and (d) $t = 406/\omega_0$. The vertical dashed-dotted line labels the position where the match condition $k_{2\omega_0} = 2k_{\omega_0}$ is satisfied. The spatial distributions of normalized kinetic energy of ions for the $J_0 = 12 \times 10^2 \, \mathrm{Am}^{-2}$ case at (e) $t = 65/\omega_0$, (f) $t = 122/\omega_0$, (g) $t = 203/\omega_0$ and (h) $t = 406/\omega_0$.

According to the observed frequency peaks and their occurrence times, the most probable nonresonant decay channels are $2\omega_0 \rightarrow \Omega_H + (2\omega_0 - \Omega_H)$ (i.e., $2\omega_0 \rightarrow 0.57\omega_0 + 1.43\omega_0$) and $2\omega_0 \rightarrow 2\Omega_H + (2\omega_0 - 2\Omega_H)$ (i.e., $2\omega_0 \rightarrow 1.14\omega_0 + 0.86\omega_0$). The produced ICQMs with frequencies $\Omega_H \simeq 0.57\omega_0$ and $2\Omega_H \simeq 1.14\omega_0$ may be heavily damped on ions, and thus their amplitudes are much smaller than that of the IBWs with frequencies $1.43\omega_0$ and $0.86\omega_0$. The region of ion heating is consistent with the one where these two nonresonant decay pairs occur. However, no ion heating is observed in the earlier time in the $J_0 = 12 \times 10^2 \, \mathrm{Am}^{-2}$ case (Figs. 2(e) and 2(f)) when these nonresonant decay pairs are absent in their corresponding spectra (Figs. 2(a) and 2(b)). Furthermore, the ions are not

heated in the $J_0 = 6 \times 10^2 \, \mathrm{Am}^{-2}$ case, while they are heated in the $J_0 = 9 \times 10^2 \, \mathrm{Am}^{-2}$ and $J_0 = 24 \times 10^2 \, \mathrm{Am}^{-2}$ cases in the region where the nonresonant decay channels appear. Therefore, it is confirmed that these nonresonant parametric decay processes are excited and give rise to the ion heating observed in the simulation.
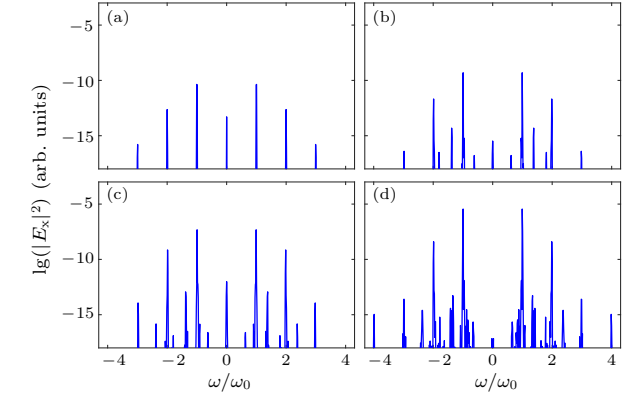
On the other hand, the IBW with frequency $1.86\omega_0$ may be excited via the resonant mode–mode coupling by the decay channel $\omega_0 + 0.86\omega_0 \rightarrow 1.86\omega_0$. The dispersion curves, i.e., the perpendicular wavenumbers versus the radial position, for the wave with frequencies $0.86\omega_0$ and $1.86\omega_0$ are plotted in Fig. 3. One can see that the selection condition of the wavenumber $k_{1.86\omega_0} = k_{\omega_0} + k_{0.86\omega_0}$ can be satisfied around

$x \simeq 0.016\,\mathrm{m}$, indicating that the wave with frequency $1.86\omega_0$ can be produced by the resonant decay process if the amplitudes of the pump waves are large enough.

At a later time as illuminated in Fig. 2(d), the amplitudes of the decay waves described above increase and a new sideband with frequency $2.43\omega_0$ appears. Similarly, the dispersion curves for the sidebands with frequencies $1.43\omega_0$ and $2.43\omega_0$ shown in Fig. 3 indicate that the selection condition $k_{2.43\omega_0} = k_{\omega_0} + k_{1.43\omega_0}$ can be satisfied around $x \simeq 0.021\,\mathrm{m}$. Thus the IBW with frequency $2.43\omega_0$ is triggered by the resonant decay channel $\omega_0 + 1.43\omega_0 \rightarrow 2.43\omega_0$. In addition, we have checked the dispersion curve for the fourth harmonic wave and have found that the selection condition $k_{4\omega_0} = 2k_{2\omega_0}$ is satisfied around $x \simeq 0.02\,\mathrm{m}$. The fourth harmonic mode detected in the $J_0 = 24 \times 10^2\,\mathrm{Am}^{-2}$ case is generated by the self-interaction of the second harmonic wave.

According to the time evolution of the frequency spectrum as well as the kinetic energy distribution of the particles, the development of the PDI spectrum in a high input power is clearly demonstrated. In this $J_0 = 12 \times 10^2\,\mathrm{Am}^{-2}$ case, the self-interaction of the injected wave excites the second harmonic mode initially. Then this generated child wave couples with the injected wave and acts as a pump wave, leading

to the generation of the other sidebands. These new sidebands couple with each other as well as the pump waves and/or act as a pump wave and thus excite more sidebands. It is found that the waves observed in the simulation are generated via the three-wave coupling process rather than the four-wave or higher order interaction.
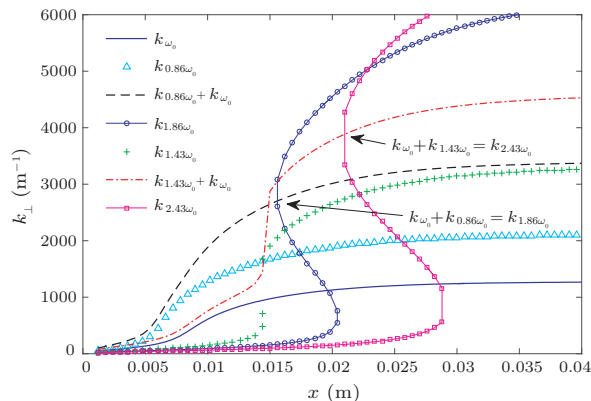

Fig. 3. Dispersion curves $k_\perp$ versus x for the IBWs with frequencies ω_0 (blue solid line), $0.86\omega_0 = 2\omega_0 - 2\Omega_\mathrm{H}$ (cyan triangles), $1.43\omega_0 = 2\omega_0 - \Omega_\mathrm{H}$ (green crosses), $1.86\omega_0$ (blue-circle solid line) and $2.43\omega_0$ (magenta-square solid line). The black dashed and red dashed-dotted lines denote $k_{\omega_0} + k_{0.86\omega_0}$ and $k_{\omega_0} + k_{1.43\omega_0}$, respectively.

Table 1. The possible decay channels in three hierarchical levels. Here m is an integer.

Levels	Decay type	Possible decay channels	Observed in simulation				
			J6	J9	J12	J24	J48
First	Resonant decay	$\omega_0 + \omega_0 \rightarrow 2\omega_0$	Y	Y	Y	Y	Y
		$\omega_0 \rightarrow \omega_2 - \omega_1$ $\omega_1 = (0.3 \sim 2.6)\omega_0\ (\omega_1 \neq m\Omega_\mathrm{H})$, $\omega_2 = (1.3 \sim 3.6)\omega_0\ (\omega_2 \neq m\Omega_\mathrm{H} + \omega_0)$	N	N	N	N	N
	Nonresonant decay	$\omega_0 \rightarrow \Omega_\mathrm{H} + (\omega_0 - \Omega_\mathrm{H})$ $0.57 \qquad 0.43$	N	N	N	N	N
		$\omega_0 \rightarrow \omega_2' - \omega_1'$ $(\omega_1' = m\Omega_\mathrm{H},\ \omega_2' = m\Omega_\mathrm{H} + 1)$	N	N	N	N	N
Second	Resonant decay	$\omega_0 + 2\omega_0 \rightarrow 3\omega_0$	Y	Y	Y	Y	Y
		$2\omega_0 + 2\omega_0 \rightarrow 4\omega_0$	N	N	N	Y	Y
		$2\omega_0 \rightarrow 0.4\omega_0 + 1.6\omega_0$	N	N	N	Y	Y
		$2\omega_0 \rightarrow 0.5\omega_0 + 1.5\omega_0$	N	N	N	N	N
		$2\omega_0 \rightarrow 0.9\omega_0 + 1.1\omega_0$	N	N	N	N	N
	Nonresonant decay	$2\omega_0 \rightarrow \Omega_\mathrm{H} + (2\omega_0 - \Omega_\mathrm{H})$ $0.57 \qquad 1.43$	N	Y	Y	Y	Y
		$2\omega_0 \rightarrow 2\Omega_\mathrm{H} + (2\omega_0 - 2\Omega_\mathrm{H})$ $1.14 \qquad 0.86$	N	Y	Y	Y	Y
		$2\omega_0 \rightarrow 3\Omega_\mathrm{H} + (2\omega_0 - 3\Omega_\mathrm{H})$ $1.71 \qquad 0.29$	N	N	N	N	N
Third	Resonant decay	$0.86\omega_0 + \omega_0 \rightarrow 1.86\omega_0$	N	Y	Y	Y	Y
		$1.43\omega_0 + \omega_0 \rightarrow 2.43\omega_0$	N	N	Y	Y	Y
		$0.86\omega_0 + 2\omega_0 \rightarrow 2.86\omega_0$	N	N	N	Y	Y
		$1.43\omega_0 + 2\omega_0 \rightarrow 3.43\omega_0$	N	N	N	N	Y
		$\omega_0 + 4\omega_0 \rightarrow 5\omega_0$	N	N	N	N	Y
		$2\omega_0 + 4\omega_0 \rightarrow 6\omega_0$	N	N	N	N	Y
		$1.43\omega_0 + 3\omega_0 \rightarrow 4.43\omega_0$	N	N	N	N	N
		$0.86\omega_0 + 3\omega_0 \rightarrow 3.86\omega_0$	N	N	N	N	N
	Nonresonant decay	$\omega_\mathrm{pump} \rightarrow m\Omega_\mathrm{H} + (\omega_\mathrm{pump} - m\Omega_\mathrm{H})$ $(\omega_\mathrm{pump} = 1.43\omega_0, 1.6\omega_0, 3\omega_0, 4\omega_0)$	N	N	N	N	N

In accordance with the selection rules of the parametric decay process, we find out the possible resonant and nonresonant decay channels and list them in Table 1 as three hierarchical levels. Whether these decay channels are observed in the simulation is also marked in Table 1. The first hierarchical level includes all the decay channels in which only the in-

jected wave acts as the pump wave, i.e., $\omega_0 \rightarrow \omega_2 \pm \omega_1$ and $\omega_0 + \omega_0 \rightarrow 2\omega_0$. In the simulation, only the decay channel $\omega_0 + \omega_0 \rightarrow 2\omega_0$ is detected in this level. Then we take the injected wave and the generated second harmonic wave as the pump waves and obtain all the possible decay channels in the second hierarchical level. In this level, the nonresonant PDIs are triggered

in simulations with the high input power. The interactions between these generated waves as well as the pump waves provide the possible decay channels in the third hierarchical level. More resonant decay channels are excited as the input power increases. The minimum frequency observed in this simulation is $0.4\omega_0$, which is determined by the selection rules of the PDI. In the $J_0 = 48 \times 10^2 \,\mathrm{Am}^{-2}$ case, the observed maximum frequency reaches the sixth harmonic of the driving frequency. The maximum value of frequency which can be reached depends on the amplitude of the injected wave.

In summary, we have illustrated that more decay channels appear in the PIC simulation of ion Bernstein wave when the input power is increased. For a low input power, the resonant mode–mode couplings dominate. The nonresonant PDIs occur at a higher input power level and lead to the ion heating. The generated child waves couple with each other as well as the injected wave and/or act as a pump wave to excite new decay channels. As a result, the frequency spectrum is broadened with the increase of the input power. During the range of the input power in our simulations, only three-wave coupling is observed, no four-wave or higher order interaction is found.

References

[1] Li J, Bao Y, Zhao Y P, Luo J R, Wan B N, Gao X, Xie J K, Wan Y X and Toi K 2001 *Plasma Phys. Control. Fusion* **43** 1227
[2] Pace D C, Pinsker R I, Heidbrink W W, Fisher R K, Van Zeeland M A, Austin M E, McKee G R and Garcia-Munoz M 2012 *Nucl. Fusion* **52** 063019
[3] Myra J R, D'Ippolito D A, Russell D A, Berry L A, Jaeger E F and Carter M D 2006 *Nucl. Fusion* **46** S455-S68
[4] Wilson J R, Bernabei S, Biewer T, Diem S, Hosea J, LeBlanc B, Phillips C K, Ryan P and Swain D W 2005 *AIP Conf. Proc.* **787** 66
[5] Rost J C, Porkolab M and Boivin R L 2002 *Phys. Plasmas* **9** 1262
[6] Pinsker R I, Petty C C, Mayberry M J, Porkolab M and Heidbrink W W 1993 *Nucl. Fusion* **33** 777
[7] Fujii T et al 1990 *Fusion Eng. Des.* **12** 139
[8] Vannieuwenhove R, Vanoost G, Noterdaeme J M, Brambilla M, Gernhardt J and Porkolab M 1988 *Nucl. Fusion* **28** 1603
[9] Porkolab M 1990 *Fusion Eng. Des.* **12** 93
[10] Porkolab M 1985 *Phys. Rev. Lett.* **54** 434
[11] Xiang N and Cary J R 2008 *Phys. Rev. Lett.* **100** 085002
[12] Xiang N and Cary J R 2011 *Phys. Plasmas* **18** 122107
[13] Jenkins T G, Austin T M, Smithe D N, Loverich J and Hakim A H 2013 *Phys. Plasmas* **20** 012116
[14] Gan C, Xiang N, Ou J and Yu Z 2015 *Nucl. Fusion* **55** 063002
[15] Kuley A, Bao J, Lin Z, Wei X S and Xiao Y 2015 *AIP Conf. Proc.* **1689** 060008
[16] Xiao J, Liu J, Qin H, Yu Z and Xiang N 2015 *Phys. Plasmas* **22** 092305
[17] He P, Gao X L, Lu Q M and Zhao J S 2015 *Chin. Phys. Lett.* **32** 115202
[18] Sun X F, Jiang Z H, Xu T, Hu X W, Zhuang G, Wang L and Wang X H 2015 *Chin. Phys. Lett.* **32** 125202
[19] Nieter C and Cary J R 2004 *J. Comput. Phys.* **196** 448
[20] Kamimura T, Wagner T and Dawson J M 1978 *Phys. Fluids* **21** 1151